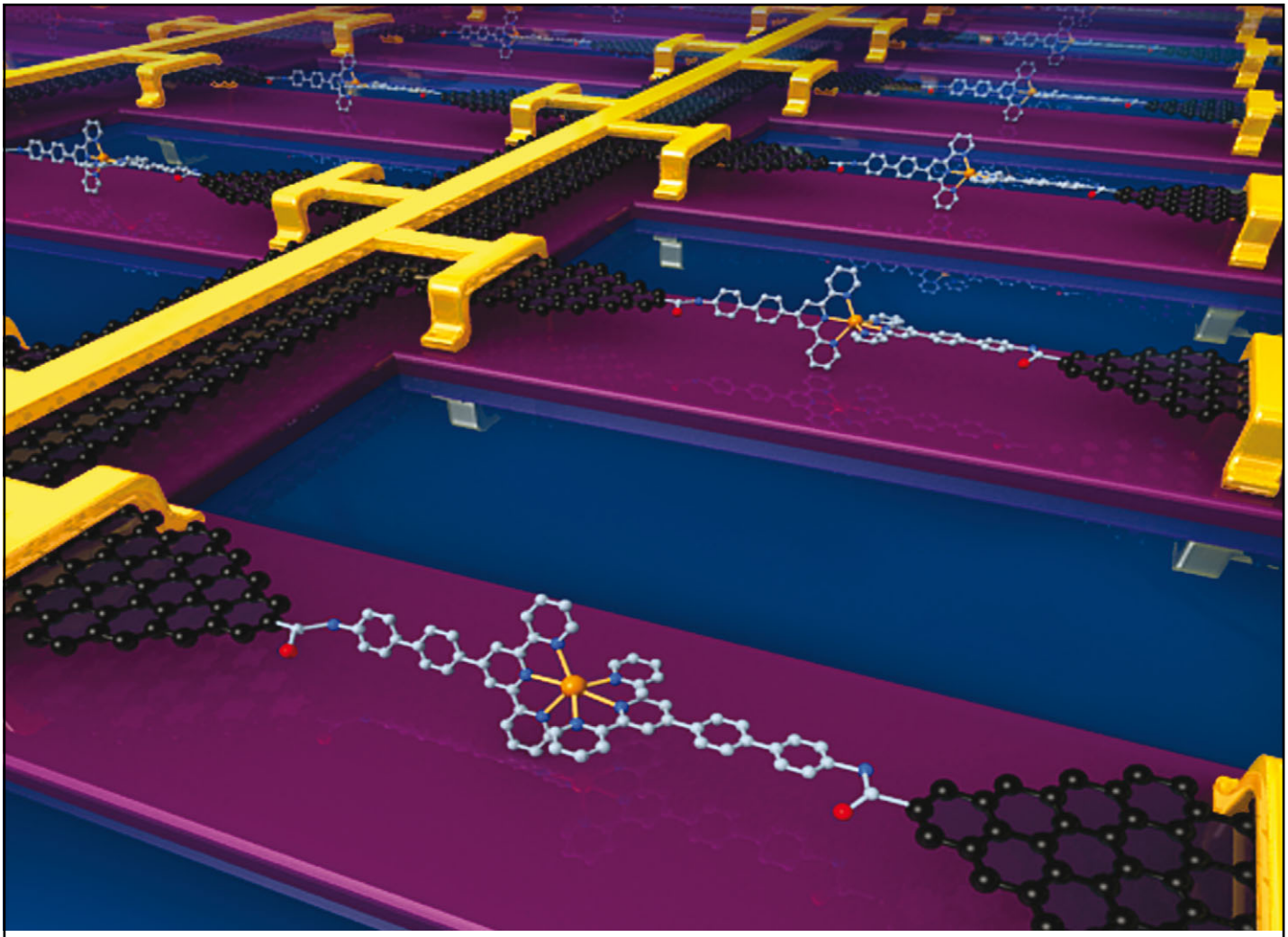

Featuring research from the group of Professor Xuefeng Guo at Institute of Physical Chemistry, Peking University College of Chemistry and Molecular Engineering, Beijing, China.

Molecule–electrode interfaces in molecular electronic devices

This review highlights the importance of molecule–electrode interfaces to the conducting properties of molecules. We summarize the strategies developed for controlling the interfacial properties and how the coupling strength between molecules and electrodes modulates the device properties.

As featured in:

See Jia and Guo,
Chem. Soc. Rev., 2013, **42**, 5642.

RSC Publishing

www.rsc.org/chemsocrev

Registered Charity Number 207890

Chem Soc Rev

RSC Publishing

TUTORIAL REVIEW

View Article Online
View Journal | View Issue

Cite this: *Chem. Soc. Rev.*, 2013, **42**, 5642

Molecule–electrode interfaces in molecular electronic devices

Chuancheng Jia[a] and Xuefeng Guo*[ab]

Received 27th December 2012

DOI: 10.1039/c3cs35527f

www.rsc.org/csr

Understanding charge transport of single molecules or a small collection of molecules sandwiched between electrodes is of fundamental importance for molecular electronics. This requires the fabrication of reliable devices, which depend on several factors including the testbed architectures used, the molecule number and defect density being tested, and the nature of the molecule–electrode interface. On the basis of significant progresses achieved in both experiments and theory over the past decade, in this *tutorial review*, we focus on new insights into the influence of the nature of the molecule–electrode interface, the most critical issue hindering the development of reliable devices, on the conducting properties of molecules. We summarize the strategies developed for controlling the interfacial properties and how the coupling strength between the molecules and the electrodes modulates the device properties. These analyses should be valuable for deeply understanding the relationship between the contact interface and the charge transport mechanism, which is of crucial importance for the development of molecular electronics, organic electronics, nanoelectronics, and other interface-related optoelectronic devices.

Key learning points

(1) The electronic structure at the molecule–electrode interface and the related charge transport mechanism.
(2) Experimental methods for studying the properties of the molecule–electrode interface.
(3) The strategies developed for regulating the properties of the molecule–electrode interface.
(4) Effects of the properties of the molecule–electrode interface on the conductance of molecular junctions.
(5) Effects of the properties of the molecule–electrode interface on the functionalities of molecular junctions.

1. Introduction

Motivated by basic scientific interests and practical applications, molecular electronics continued to undergo a very rapid growth over the past decade (ref. 1–4 and references therein). This is because organic molecules have both ultra-small dimensions and an overwhelming degree of diversity and functionality, with essentially full control over molecular design through chemical synthesis. Therefore, molecular electronics is supposed to provide the inherent scalability into the nanometer region, low production costs using self-assembly procedures and the possibility to integrate complex functions at the same time. To this end, discrete approaches have been developed to form molecular transport junctions (MTJs), including the ones based on nanogaps fabricated by shadow mask evaporation, mechanical break junction technique, scanning probe technique, electroplating, lithographic method, and electromigration, and others based on nanopores, mercury drop contacts, crossbar nanostructures, and template-prepared nanowires (ref. 1–4 and references therein). In spite of these remarkable achievements, these conceptually simple MTJs—consisting of only one or a small collection of molecules—are still not fully understood due to a number of different fundamental issues such as the fabrication process, the device stability, the contact geometry, the molecular conformation, the exact number of molecules to be tested, and the measurement condition. Work in this area is still focused on the construction, measurement, and understanding of the electronic and photonic responses of the nanoscale circuits in which molecular systems play an important role as pivotal elements.

[a] *Center for NanoChemistry, Beijing National Laboratory for Molecular Sciences, State Key Laboratory for Structural Chemistry of Unstable and Stable Species, College of Chemistry and Molecular Engineering, Peking University, Beijing 100871, P.R. China. E-mail: guoxf@pku.edu.cn*
[b] *Department of Materials Science and Engineering, College of Engineering, Peking University, Beijing 100871, P.R. China*

As demonstrated by the comprehensive set of the aforementioned experiments, a formidable challenge in molecular electronics is to understand charge transport of single or a few molecules sandwiched between electrodes, of fundamental importance to the realization of practical molecular electronic devices.[5] This requires the fabrication of reliable devices, which depend on several factors including the testbed architectures used, the molecule number and defect density being tested, and the nature of the molecule–electrode interface. On the basis of significant progresses achieved in both experiments and theory over the past decade, in this *tutorial review*, we focus on new insights into the influence of the nature of the molecule–electrode interface, the most critical issue hindering the development of reliable devices, on the conducting properties and functionalities of MTJs. We start with the introduction of the electronic structures at the molecule–electrode interface. We then overview the strategies used for studying the interactions between the molecules and the electrodes. Finally, we detail the effects of the different molecule–electrode interfaces on molecular conductance and device functionalities, respectively. However, this research field is a diverse and rapidly growing one. Having limited space and references, we will only be able to cover some of the major contributions with the most general applicability and highlight some important aspects, which were neglected in most previous reviews. Fortunately, there are a number of excellent previous review papers in the literature covering various aspects of molecular electronics, which can amend these deficiencies (ref. 1–6 and references therein).

2. The electronic structures at the molecule–electrode interface

In MTJs, charges are firstly injected from one electrode into the molecules and then collected by the other electrode. Both charge injection and collection occur across the molecule–electrode interfaces. Therefore, it is obvious that the interfacial properties between the molecules and the electrodes play an important role in the electrical characteristics of molecular devices. Previous studies have shown that changing the contact types between the molecules and the electrodes can tune their coupling strength, control the charge transport mechanism and/or improve the stability of molecular devices.[1,5] In this section, we will introduce the types of the molecule–electrode interactions and corresponding charge transport mechanisms.

2.1 The types of the molecule–electrode interactions

The coupling strength between electrons in the molecules and those in the electrodes, which can be physically depicted as an energy barrier between the molecules and the electrodes, is one of the most important properties of the molecule–electrode interface.[6] This coupling has a relationship with both the intramolecular coupling of the molecules and the coupling between the terminal of the molecules and the electrodes (denoted the intermolecular coupling). For the intramolecular coupling, in most cases saturated carbon atom connections can be used for the weak coupling and a direct π-conjugated bond can lead to the strong coupling. For the coupling between the terminal of the molecules and the electrodes, the interaction types at the molecule–electrode interface play an important role.[1] In general, physisorption of the molecules on the surface of the electrodes, which is only through a weak van der Waals interaction, leads to a weak coupling, while chemisorption, due to the formation of the strong covalent bonds between the anchoring groups of the molecules and the electrodes, results in a strong coupling. If the molecules are charged, other possible interactions, such as rearrangement of electron density, partial charge transfer, and attraction through image forces, could be further involved in the interface formation.[1] Therefore, due to the complexity of the interface formation it is crucial to know the exact way in which the interface is formed.

2.2 Charge transport mechanisms in general

To accurately define the coupling strength, we should compare two physical parameters: the coupling parameter (Γ) and the addition energy (U). The former (Γ) is defined as the

Chuancheng Jia

Mr Chuancheng Jia received his BS degree in chemistry from Shandong University in 2009 on fuel-cells and photocatalysis. He is currently working toward a PhD degree in Chemistry at College of Chemistry and Molecular Engineering, Peking University, Beijing, under the guidance of Prof. Xuefeng Guo. His research interest includes single-molecule switches and dynamics.

Xuefeng Guo

Dr Xuefeng Guo received his PhD in 2004 from the Institute of Chemistry, Chinese Academy of Science, Beijing. From 2004 to 2007, he was a postdoctoral research scientist at the Columbia University Nanocenter. He joined the faculty as a professor under "Peking 100-Talent" Program at Peking University in 2008. In 2012, he won the national science fund for distinguished young scholars of China. His research is focused on functional nanometer/molecular devices.

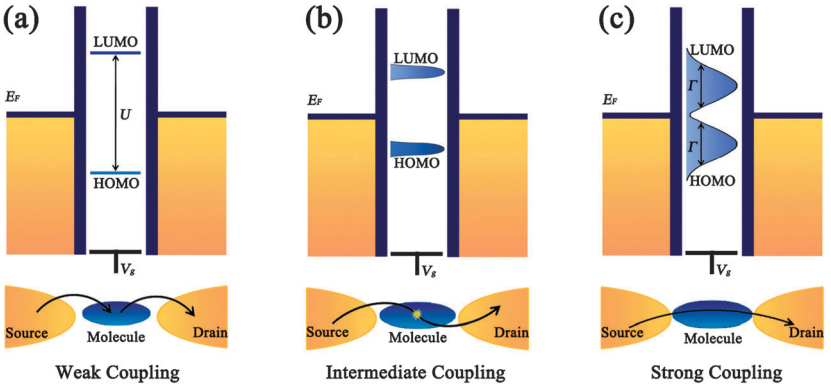

Fig. 1 Schematic representation of the energy levels and charger transport processes of MTJs with the different coupling strengths between the molecules and the electrodes. (a) In the weak coupling regime, the HOMO and LUMO of molecules are well defined, and electron transport takes place in a two-step process. (b) In the intermediate coupling regime, the HOMO and LUMO become broader and closer to Fermi energy of electrodes (E_F), and electron transport through the molecules interacting with the electrons on the molecules. (c) In the strong coupling regime, a large broadening of molecular energy levels occurs, and electrons move from the source to the drain through a one-step process.

broadening of the energy level in the molecules (which is relatively narrow in the weak coupling case or in isolated molecules in the gas phase) induced by the coupling between the molecules and the electrodes. The latter (U) is the difference between the energy needed to take one electron from the highest occupied molecular orbital (HOMO) of the system (U^{N-1}–U^N) and the energy obtained by injecting one electron to the lowest unoccupied molecular orbital (LUMO) of the system (U^N–U^{N+1}), where U^N is the total energy of the system with N electrons. Due to the strong influence of the electrodes on the molecules, the entire device should be taken as the fundamental unit for the calculation of the addition energy, not the isolated molecule. When $\Gamma \ll U$, the system is in the weak coupling regime, whereas for $\Gamma \gg U$ the system is in the strong coupling regime.

In the weak coupling regime ($\Gamma \ll U$), the wavefunctions of molecules have little mixing with the electronic states of electrodes (Fig. 1a), and no charge transfer or integer charge transfer between the molecules and the electrodes occurs. For electron transport in this case, the electrons firstly hop from one electrode to the molecule, which has matched energy levels at a proper position, and then hop to the other electrode, through a two-step process (Fig. 1a). At low temperature, without matched energy levels, electron transport is blocked unless the gate voltage (V_g) brings the energy levels of molecules to the resonance with the Fermi energy (E_F) of electrodes, or bias voltages are high enough to bring E_F to the molecular energy levels. This phenomenon is also called the Coulomb-blockade, which forms classic Coulomb diamonds in differential conductance maps.

For the strong coupling ($\Gamma \gg U$), the electronic states of molecules and electrodes are significantly overlapped and partial charger transfer between the molecules and the electrodes occurs, which leads to a great broadening of the energy levels of molecules (Fig. 1c). Therefore, the electrons could efficiently transport from one electrode to another through a one-step coherent process without stopping on the molecules. Correspondingly, the Coulomb blockade map breaks down, and the gate voltage (V_g) has little effect on the transport current.

In the intermediate coupling regime, the molecular energy levels are partially broadened (Fig. 1b). During electron transport, the transferred electrons can be affected by the electrons on the molecules. When there is an unpaired electron on the molecules, electrons passing through the molecules can reverse the spin state of the unpaired electron and spin screening occurs. This screening opens up new transport channels and zero-bias Kondo resonance takes place below a certain temperature. In addition to these, a co-tunneling process can also occur in this regime, in which one electron tunnels into the LUMO of the molecule with another electron simultaneously tunneling out of the HOMO, and thus leaves the molecule in the excited state.

On the basis of the above-discussed mechanisms, it is reasonable that controlling the coupling strength between the molecules and the electrodes affords the required charge transport properties of MTJs. In this regard, accurate contacts between the molecules and the electrodes at the atomic level are needed for realizing the precise interface coupling control.

3. Strategies for studying the interactions between the molecules and the electrodes

As discussed above, the bonding type, the coupling strength and related energy level positions between the molecules and the electrodes are the most important interface characteristics for MTJs. Here we summarize the commonly-used experimental methods for the study of the interfacial properties of molecular junctions, especially single-molecule junctions.

3.1 Bonding characteristics: inelastic electron tunneling spectroscopy

Inelastic electron tunneling spectroscopy (IETS), which is associated with the interaction between the transporting electrons

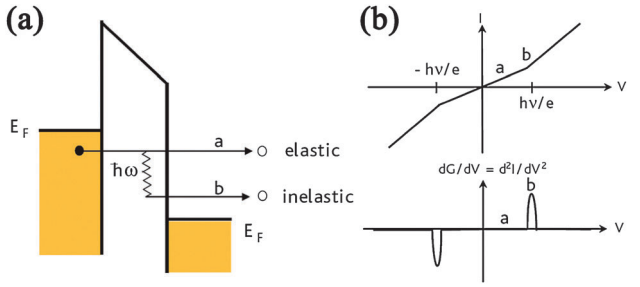

Fig. 2 Schematic presentation of inelastic electron tunneling spectroscopy (IETS). (a) Energy band diagram for a tunnel junction. (b) Corresponding $I(V)$ and d^2I/dV^2 characteristics. Reproduced with permission from ref. 7. Copyright © 2008 Elsevier Ltd.

and the molecular vibrations (phonons), is now being used as an important analytical tool for the investigation of molecular junctions.[7] With small applied bias, the electron can directly tunnel through the molecules from the occupied state of one electrode to the empty state of the other without any loss of energy, which is elastic tunneling. This affords a linear relation between the current and the applied bias. When the applied bias energy (eV) is larger than the molecular vibration energy ($\hbar\omega$), the electron can lose a quantum of energy to excite the molecular vibration (Fig. 2a). This opens a new inelastic tunneling channel for electrons. Correspondingly, the overall tunneling probability is increased with a kink at the current-bias plot (Fig. 2b). Such changes can be reproducibly observed as a peak in the second derivative of the current–voltage (I–V) curves (d^2I/d^2V). This plot of d^2I/d^2V *versus* V is referred to as IETS (Fig. 2b). For experimental measurements, due to the weak signal of inelastic tunneling, the lock-in second harmonic detection technique with an AC modulation is used for the measurement of the d^2I/d^2V *versus* V plot. In addition, due to the thermal broadening effect, the IETS measurements should be carried out at cryogenic temperatures.

For studying the interactions between the molecules and the electrodes, IETS is useful in investigating the bonding situations for the molecule–electrode linkages by the features of the corresponding vibrational peaks. The breaking and the formation of chemical bonds at the contacts can be monitored by the decrease and the growth of the vibrational peaks. During the stretch of molecular junctions, the position shift of the corresponding vibrational peaks, which correspond to the changes in the bond length, can be used to study the bond strength at the contacts.[8] Additionally, the changed molecular electronic structures, which are due to the coupling with the electrodes, can also be investigated by IETS based on the changes in the characteristic vibrational peaks.

3.2 Energy levels: transition voltage spectroscopy and thermoelectricity

The position and broadening of the molecular energy levels, which can be controlled by the interfacial interaction at the contacts, are the most important factors for electron transport in molecular junctions. Transition voltage spectroscopy (TVS) and thermoelectricity are effective experimental methods used to study such characteristics of the energy levels in molecular junctions.

TVS, which exploits the nonlinear current–voltage characteristics of molecular junctions, is a powerful tool to investigate the energy offset between the Fermi energy of the electrodes and the closest molecular energy levels. For electron transport in molecular junctions, it can be simplified as electron tunneling through a barrier.[9] In the zero-bias limit, the tunneling barrier has a rectangular shape (Fig. 3a), and the current–voltage relationship is

$$I \propto V \exp\left(-\frac{2d\sqrt{2m_e\phi}}{\hbar}\right)$$

where d is the barrier width, m_e is the electron effective mass, and ϕ is the barrier height. Thus, $\ln(I/V^2)$ is proportional to $\ln(1/V)$. When the applied bias is larger than the barrier height, the shape of the tunneling barrier is transformed to be triangular (Fig. 3a), and the current–voltage relationship is

$$I \propto V^2 \exp\left(-\frac{4d\sqrt{2m_e\phi^3}}{3\hbar qV}\right)$$

Here, q is the electronic charge. Then, the relation between $\ln(I/V^2)$ and $1/V$ is linear. Accordingly, as the shape of the tunneling barrier changes from rectangular to triangular with the increasing bias, the charge transport mechanisms are transformed from a direct tunneling to a field emission. From the plot of $\ln(I/V^2)$ against $1/V$ (Fowler–Nordheim (F–N) plot), the transition voltage (V_{trans}) can be obtained (Fig. 3b), which is the effective energy height for electron transport and corresponds to the energy offset between the electrode Fermi level and the closest molecular energy level. It should be mentioned that V_{trans} is dependent on the contact symmetry. If the molecules do not possess central symmetry, the molecular dipole results in an electrostatic potential, which could create an asymmetry in the two metal–molecule contacts. Such contact asymmetry can lead to rectification in molecular junctions because of unequal voltage drops at the two molecule–electrode interfaces.[9]

For a more real mode of electron transport, the resonant tunneling is considered as the viewpoints rather than the tunneling barrier. Araidai and Tsukada[9] reported that V_{trans} in the F–N plot can take place when a certain amount of the tail of the resonant peak enters the bias window (Fig. 3b). The resonant peak also corresponds to the closest molecular energy level of molecular junctions. Therefore, TVS is a reliable method to study the energy level relationship between the electrode Fermi level and closest molecular orbital.

Thermoelectricity, which measures the voltage difference created across a molecular junction in response to an applied temperature, can be used to determine the conduction types of molecular junctions (either p-type or n-type) and whether the HOMO or LUMO level of molecules is closer to the Fermi level of the electrodes.[10] The relative position between the molecular

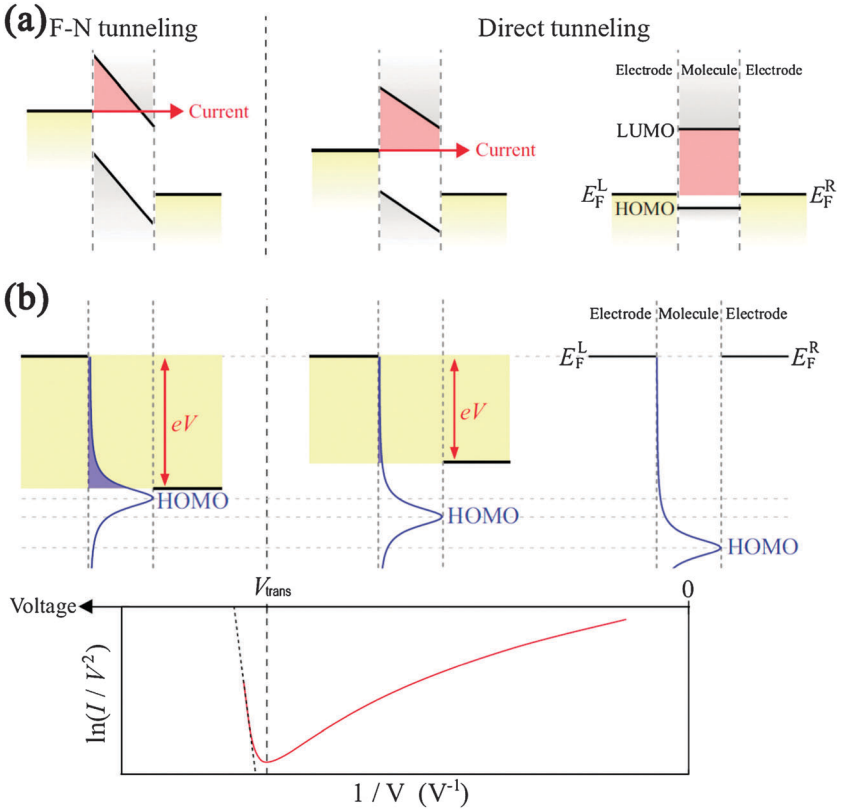

Fig. 3 Schematic diagrams of the conventional models to qualitatively explain the transition of the F–N curves. (a) The shapes of the tunneling barrier. (b) The corresponding resonant tunneling mechanisms. Reproduced with permission from ref. 9. Copyright 2010 American Physical Society.

energy levels and the electrode Fermi level can be determined by the thermoelectric Seebeck coefficient ($S_{junction}$) of molecular junctions (Fig. 4). The relationship between $S_{junction}$ and the transmission function ($\tau(E)$) can be given by the Landauer formula:

$$S(E_F) = -\frac{\pi^2 k_B^2 T}{3e}\frac{\partial \ln(\tau(E))}{\partial E}\bigg|_{E=E_F}$$

where k_B is the Boltzmann constant, T is the average temperature of the electrodes and E_F is the Fermi level of the electrodes. From the Landauer formula, we also know that the conductance ($G_{molecule}$) of molecular junctions can be related to the transmission function in the zero-bias limit as

$$G_{molecule} = \frac{2e^2}{h}T(E)\bigg|_{E=E_F}$$

with the values of $S_{junction}$ and $G_{molecule}$, the specific difference between HOMO or LUMO levels and E_F can be obtained.[10]

For experimental measurements (Fig. 4a), one side of the electrodes is usually made to come into contact with a large thermal reservoir to maintain the stability of the temperature, while the other side of the electrodes is heated with a heater to a desired temperature to create a temperature difference (ΔT) between the two electrodes. The thermoelectric current (ΔI) through the junction at zero bias voltage and the output voltage (ΔV) at zero current can be measured. The Seebeck coefficient of molecular junctions is given by $S_{junction} = S_{electrode} - \Delta I/G\Delta T$ with thermoelectric current (ΔI), and $S_{junction} = S_{electrode} - \Delta V/\Delta T$ with thermoelectric voltage (ΔV), where $S_{electrode}$ is the Seebeck coefficient of the electrode material. Fig. 4b shows the experimental Seebeck coefficient of Au–BDT–Au junctions, which is in excellent consistence with the theoretical predictions. When $S_{junction}$ is positive (p-type), the HOMO level is closer to E_F of the electrodes; when $S_{junction}$ is negative (n-type), the LUMO level is closer to E_F.

The terminal groups of the molecules have a great effect on the conduction characteristics of molecular junctions. Using thermoelectric measurements, Widawsky *et al.*[11] have studied the thermoelectric features of amine-terminated and pyridine-terminated molecular junctions. They found that amine-terminated molecular junctions have a positive Seebeck coefficient related to the HOMO resonance closer to E_F, while pyridine-terminated molecular junctions have a negative Seebeck coefficient with conduction through the LUMO.

3.3 Mechanics: the break junction technique

The force measurement, which uses the break junction techniques to monitor the force characteristics of molecular junctions based on the related molecular conductance during the junction formation and evolution, is an efficient way to study the bonding strength at the contact interface of molecular junctions. Using gold electrodes as an example, the formation of

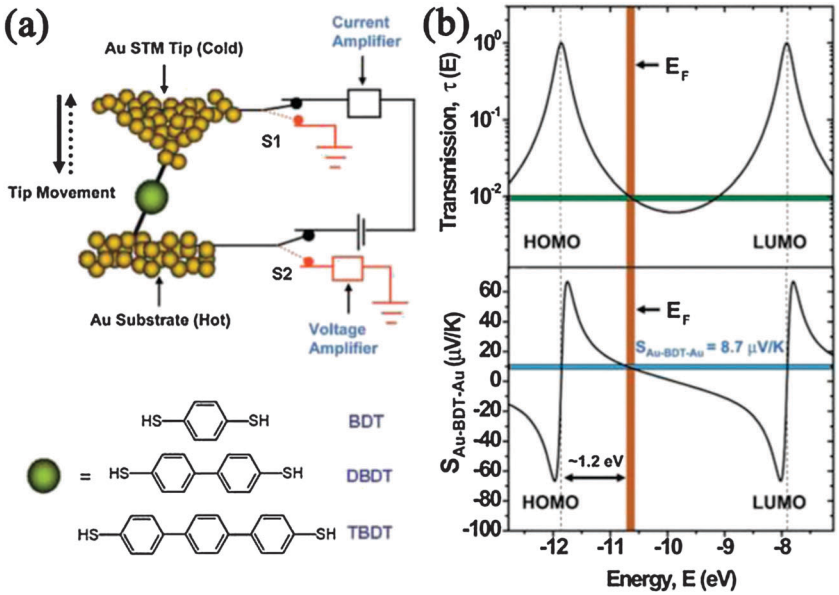

Fig. 4 (a) Schematic description of the experimental setup based on an STM break junction. (b) Relating the experimental Seebeck coefficient of Au–BDT–Au with the theoretical predicted transmission function and the position of the Fermi level. Reproduced with permission from ref. 10. Copyright 2007 American Association for the Advancement of Science.

Au–molecule–Au junctions occurs as follows: at the initial stage, the mechanical elongation of Au–Au nanocontacts shows the stepwise decrease in the conductance until a long plateau is formed with a conductance of $1G_0$ ($G_0 = 2e^2/h$ is the conductance quantum), which corresponds to the single atom contact. Further stretching leads to the breakdown of Au junctions and then the conductance drops to zero when no molecules are present. However, if a target molecule is trapped in the gap of Au electrodes, an additional conductance plateau of Au–molecule–Au junctions can be observed until complete breakdown of the junctions. During such stretching of the junctions, rich characteristics of molecular junctions can be obtained, such as the quantum conductance, the bond rupture force, the tensile elongation, and so on.

The bond rupture force is the force required for the rupture of electrode–molecule–electrode junctions, which usually occurs at the contact bonds formed between the terminals of the molecules and the atoms of the electrodes. Therefore, the binding energy of the contact bond and the corresponding coupling strength between the molecules and the electrodes can be detected. Recently, a conducting atomic force microscopy (C-AFM) break junction technique was used by Frei *et al.*[12,13] to measure single-molecule bond rupture forces (Fig. 5a). A new two-dimensional histogram technique (Fig. 5b), which is the statistics of all the available conductance and force traces, is introduced to reliably achieve the bond rupture forces. On the basis of the histogram, the breaking forces for molecular junctions bridged by amine, methylsulfide, and diphenylphosphine-terminated molecules are obtained at about 0.6, 0.7, and 0.8 nN, respectively, which correspond to the breaking of Au–N, Au–S, and Au–P donor–acceptor (D–A) bonds. For thiol terminated molecules, the changed conductance and force values support the notion that a strong covalent S–Au bond may cause the local structural rearrangement in soft Au electrodes under stress. However, on average the rupture forces in these junctions are smaller than the 1.4 nN rupture force for the single Au atom contact.

The break junction technique can also be used to evaluate the stability and natural lifetime of electrode–molecule contacts in molecular junctions. From the conductance–time curves of molecular junctions with certain elongation speeds (v_d), the lifetime (τ_B) and elongation length (L) of the junctions, which are related to the plateau length of the stretched single-molecule junctions, could be achieved. For example, by using a mechanical self-breaking method (Fig. 5c), Tsutsui *et al.* investigated the thermodynamic stability of single-molecule junctions with thiol and amine anchoring groups.[14] Due to the force-accelerated thermoactivated breakdown of single-molecule junctions during the stretching, the lifetime decreases and the elongation length increases with the increasing elongation speed at $v_d > 0.06$ nm s^{-1}. However, when the elongation speed is low enough, $v_d < 0.06$ nm s^{-1}, the self-breaking is under negligible forces with L approaching zero and constant τ_B. Therefore, the natural lifetime, which is the survival time of molecular junctions that fracture by thermal fluctuations with zero-force, can be deduced from τ_B at a lower elongation speed. They found that for 1,4-benzenediamine and 1,4-benzenedithiol molecular junctions, the natural lifetime of Au–S contacts is five orders of magnitude longer than that of Au–NH_2 contacts.

The local heating at the molecule–electrode contacts, which is due to the electron–phonon and electron–electron scattering processes during charge transport, can also be detected by force measurements of single-molecule junctions. By measuring the

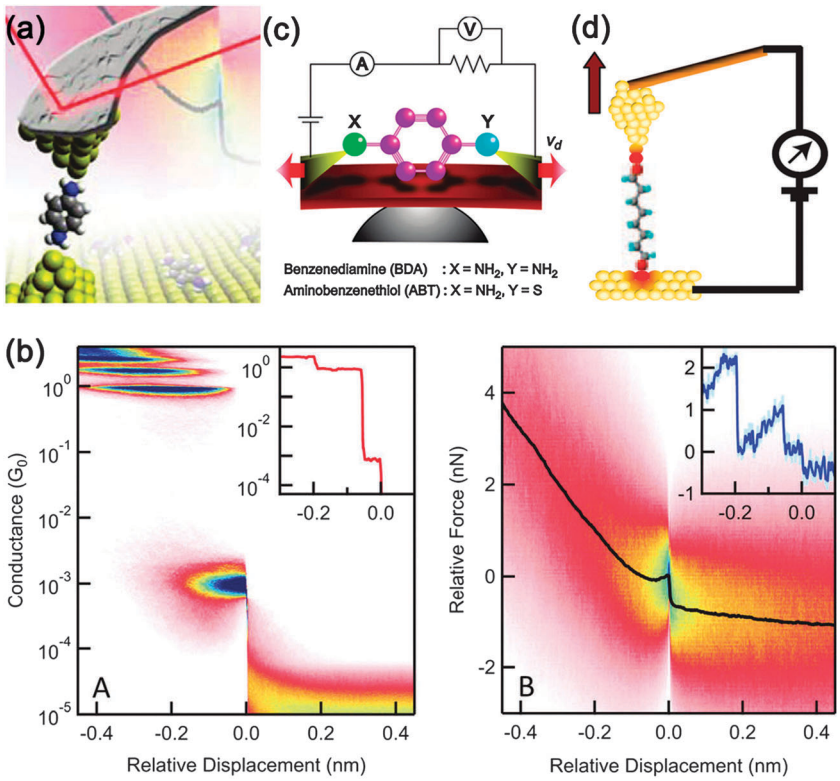

Fig. 5 Force measurements with break junction techniques. (a) C-AFM break junction used for single-molecule bond rupture force measurements. (b) Two-dimensional conductance (left) and force (right) histograms of 1,4-diaminobutane Au molecular junctions constructed from over 10 000 times measurements. Insets: a sample conductance trace and force trace acquired from one measurement. Reproduced with permission from ref. 12. Copyright 2011 American Chemical Society. (c) Mechanical self-breaking method used for thermodynamic stability measurements. Reproduced with permission from ref. 14. Copyright 2009 American Chemical Society. (d) STM break junction used to measure the local heating at the molecule–electrode contacts. Reproduced with permission from ref. 15. Copyright 2008 Nature Publishing Group.

elongation length (L) of scanning tunneling microscopy (STM) break junctions as a function of the stretching rate and temperature (Fig. 5d), Huang *et al.*[15] studied the local heating in single molecules as a function of the applied bias and the molecular length. During the thermally-activated process of the bond breaking at a certain stretching speed, the relationship between the effective local temperature (T_{eff}) of molecular junctions and the elongation length (L) can be written as

$$L = \frac{E_{\mathrm{b}}}{x_{\beta}k_{\mathrm{s}}} + \frac{k_{\mathrm{B}}T_{\mathrm{eff}}}{x_{\beta}k_{\mathrm{s}}}\ln\left(\frac{x_{\beta}k_{\mathrm{s}}t_{\mathrm{D}}}{k_{\mathrm{B}}T_{\mathrm{eff}}}v\right)$$

where E_{b} is the breaking energy barrier, x_{β} is the average thermal bond length along the stretching direction until rupture, t_{D} is the diffusion relaxation time, k_{s} is the effective spring constant, k_{B} is the Boltzmann constant, and v is the stretching rate. Therefore, with known v, T_{eff} of molecular junctions can be directly deduced from L. As most of the breakings occur at the contact point, T_{eff} at the contacts and related interfacial scattering conditions during charge transport can be obtained. They found that T_{eff} of molecular junctions first increases with the applied bias, and then decreases after reaching a maximum. At a fixed bias, T_{eff} decreases with the increasing molecular length.

4. Effects of different molecule–electrode interfaces on molecular conductance

As discussed above, the electronic structures of molecule–electrode interfaces have a great effect on the electrical characteristics of molecular junctions, especially the molecular conductance. From the Landauer formula, the conductance (G) of molecular junctions can be described as[1]

$$G = \frac{I}{V} = \frac{2e^2}{h}T_{\mathrm{L}}T_{\mathrm{R}}T_{\mathrm{mol}}$$

where I is the current through the junction, V is the applied bias, and T_{L}, T_{R} and T_{mol} are the transmission coefficients of the left interface, the right interface and the molecule, respectively. For tunneling transport, when the Fermi levels of the electrodes lie in the gap between the HOMO and LUMO of the molecules, both the interfacial coupling strength and the energy level offset between the electrodes and the molecules significantly influence the conductance of molecular junctions. For resonant transport, however, the Fermi levels of the electrodes are resonant with the molecular energy levels; the conductance depends only on the contact resistance due to the different coupling strength. Therefore, to realize controlled charge transport in molecular junctions, both the coupling

strength and the energy level alignment at the interfaces between the electrodes and the molecules should be precisely controlled. Here, we systematically summarize the strategies developed for the regulation of the molecule–electrode interfaces and thus related electrical properties of molecular junctions, such as the use of different electrodes, molecular anchoring groups, intramolecular connections, and external conditions.

4.1 Different electrodes

The proper choice of the electrode materials is one of the most important parameters to build good molecule–electrode contacts and regulate the interfacial characteristics of molecular junctions. To date, different fabrication methods have been developed to create molecular junctions,[2] such as C-AFM, STM break junction, MCBJ (mechanically controllable break junction), electromigration, lithographic methods, transfer printing, soft contact lamination, direct evaporation and indirect evaporation. These molecular junction fabrication methods make it possible to construct molecular junctions using different electrode materials.

Metallic gold electrodes, which have a good stability, high conductivity, good fabricability and well-developed self-assembling methods with molecules, have been widely used in molecular junctions. When gold electrodes are replaced by other metallic materials, the interfacial energy level alignment and the coupling strength between the electrodes and the molecules could be adjusted. For example, when Ag, Pd, Au, and Pt are used as electrodes,[16] which have work functions of 4.26 eV, 5.12 eV, 5.10 eV and 5.65 eV, respectively, the Fermi energy of the electrodes reduces with the increase in work function. Correspondingly, the energy offsets between the Fermi energy of the electrodes and the HOMO of the molecules decrease, which can be confirmed using transition voltage spectroscopy (TVS) with reduced transition voltages (V_{trans}) for hole tunneling systems with HOMO dominating the conduction of molecular junctions. In contrast, for LUMO-mediated tunneling systems, the increase in the electrode work functions might enlarge the energy level alignments between the Fermi level of the electrodes and the LUMO of the molecules. Then, the corresponding V_{trans} from TVS increases. When molecular junctions are formed from asymmetric electrodes, with the increase in the electrode work functions, it is reasonable that the reduced tunneling barrier and enhanced conduction for tunneling systems with HOMO dominating charge transport can be observed from the asymmetry current–voltage characteristic curves of molecular junctions.[17]

In addition, the orbital characteristics of the electrode atoms also have a great effect on the electronic coupling between the molecular headgroup and the electrode (and thus the conductance of molecular junctions). Ko *et al.*[18] used Au, Pd and Pt as electrodes in thiol (–SH) or isothiocyanate (–NCS)-terminated molecular junctions to study the effects of the electrode materials on the interfacial electronic coupling and the conductance of molecular junctions. As Au is a group 11 element with strong s-orbital characteristics, σ bonding can be formed at the contact between the Au electrodes and the headgroups of molecules in most cases, such as –S–Au and –NCS–Au. On the other hand, because Pd and Pt are group 10 elements with significant d-orbital characteristics, π contributions are expected at the contact especially for –NCS headgroups with a strong π character, which will generate an additional channel for electron transport. The quantitative sulfur–metal bond orders of –S–Au, –S–Pt, –NCS–Au, –NCS–Pd, and –NCS–Pt using Mayer 2-center bond-order calculations are found to be 0.837, 1.280, 0.393, 0.660 and 0.739, respectively. Further analysis of the headgroup-metal bond orders reveals that the relative contributions of π to σ characters for the cases of –NCS–Pd and –NCS–Pt were 1/3 and 1/2, respectively. These results show a good correlation with the measured contact conductance, which demonstrates the stronger electronic coupling at the contacts and higher conductivity of molecular junctions in Pd and Pt electrode systems.

In some cases, the different conductance can be observed in the same molecular junction system due to the different headgroup–substrate binding geometries, which in general play a significant role in the molecular conductance.[18] For molecular junctions with Au–S contacts made by a break junction technique, when one headgroup is connected to 3-fold hollow sites of the substrate and the other at atop sites (denoted atop–hollow), a high conductance of molecular junctions can be obtained, while molecular termini sitting on two atop sites (atop–atop) results in low conductance. Because molecular junctions are produced by pulling the gold atoms out of the electrodes using break junction techniques, which result in at least one atop geometry at the junctions, hollow–hollow configurations cannot be formed. It should be mentioned that the electrode orientations also have a great effect on the interfacial coupling. This is because different electrode orientations have different band structures. Sen and Kaun[19] attributed the observed binary (high/low) conductance in thiol-terminated single-molecular junctions to the distinct electrode orientations. On the basis of the theoretical calculations, they found that the electrode–molecule coupling of molecular junctions is stronger for Au electrodes with the (100) direction than that with the (111) direction.

Although metallic materials, especially gold, have been widely used as the electrodes in molecular junctions, the high atomic mobility for gold and the low chemical stability for those with low work functions may lead to the destruction of molecular junctions upon oxidation or electromigration. In order to realize more stable and controllable contacts for molecular electronics, sp^2-hybridized carbon electrodes have been developed to form molecular junctions with nonmetallic contacts. For example, all-carbon molecular junctions with enhanced stability were fabricated by Yan *et al.*[20] in high yield using self-assembled monolayers (SAMs) sandwiched between two carbon conductors (Fig. 6a). Through an electrochemical radical reaction, three molecular layers (fluorene (FL), nitroazobenzene (NBA) and *n*-octylamine (C8N)) were covalently attached to the bottom graphitic carbon substrates made from pyrolyzed photoresist films (PPF). These covalent C–C surface

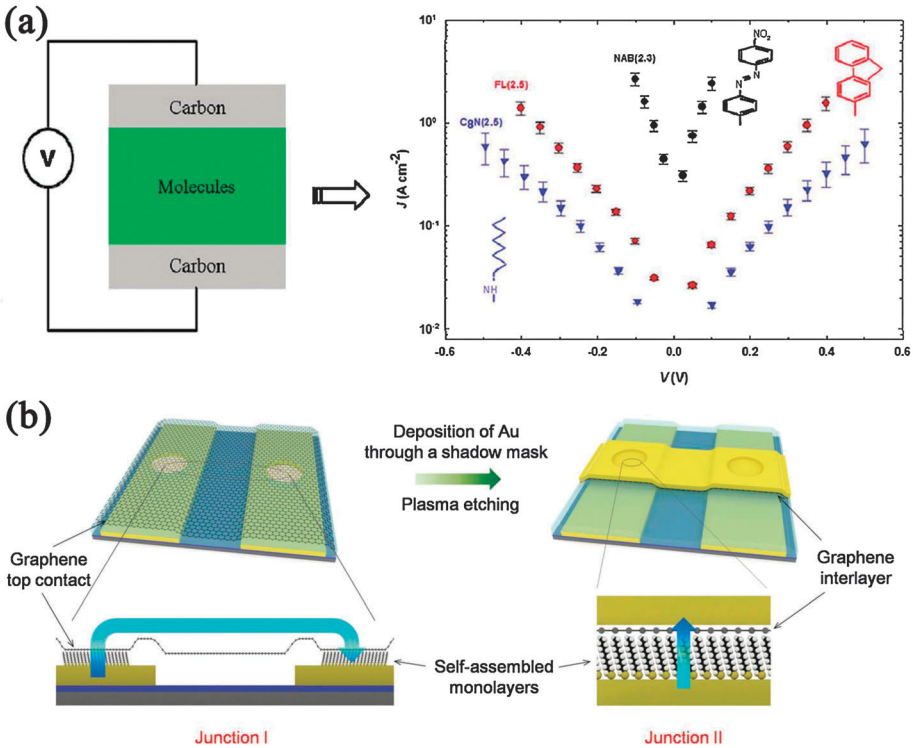

Fig. 6 (a) Schematic representation of an all-carbon molecular junction (left). The molecules used and related current density–voltage (*J–V*) curves of molecular junctions studied (right). Reproduced with permission from ref. 20. Copyright 2011 American Chemical Society. (b) Two types of molecular junctions: CDG films used as a top contact electrode (left) and the conductive interlayer (right). Reproduced with permission from ref. 21. Copyright 2012 Wiley-VCH Verlag GmbH & Co. KGaA.

bonds result in the strong molecule–electrode electronic coupling. Then, they used electron beam-deposited carbons (e-C), which are disordered and sp^2-hybridized, as a nonmetallic top contact. The energy level offsets between the electrode Fermi level and the frontier molecular orbitals determined using ultraviolet photoelectron spectroscopy (UPS) were found to be 1.16, 1.52, and 1.96 eV for NAB, FL, and C8N, respectively. These values follow the trend of the junction conductance shown in Fig. 6, with a smaller energy level offset corresponding to the higher junction conductance. In comparison with Cu top contact junctions, the conductance of e-C top contact junctions is much lower, which is due to the differences in the surface density of states (DOS) in the electrode materials. Similarly, graphene, an atomically thin layer of sp^2-hybridized carbon atoms arranged in a honeycomb lattice, can also be used as soft top contacts for molecular junctions as demonstrated by Li *et al.*[21] They proved that chemically derived graphene (CDG) films can be directly used as top contact electrodes or as the conductive interlayer to protect SAMs from invasive metal contacts for making ensemble molecular junctions (Fig. 6b).

Among carbon materials, single-walled carbon nanotubes (SWNTs) are unique because in addition to their high electrical conductivity and good thermal stability, they have the nature of a one-dimensional (1D) structure, which perfectly matches the size with single molecules. This strongly suggests that SWNTs could be used to prepare nanoscale electrodes for creating single-molecule junctions. To do this, recently we have successfully developed a reliable process to prepare nanogapped SWNT electrodes by oxygen plasma ion etching through a polymethylmethacrylate (PMMA) mask defined with e-beam lithography (Fig. 7a).[22] Due to the strong oxidative etching condition, carboxylic acid groups are expected to dominate the cut ends of SWNT electrodes. Then, individual molecules with amine anchoring groups can be covalently attached to the carboxylic acid-functionalized electrodes *via* the formation of robust amide bonds, thus forming a new type of single-molecule junctions (Fig. 7b). It is due to well-defined covalent bonds between the molecules and the electrodes that these resulted single-molecule junctions are stable enough to endure chemical treatments and external stimuli, thus ensuring the investigation of the intrinsic properties of molecules and even installing new functionalities.[4] Most recently, we have developed another efficient method, called ''Dash-line Lithography (DLL)'', to build single-molecule junctions using point contacts made from graphene as electrodes in high yields (~50%) (Fig. 7c).[23] This approach overcomes the problems that SWNT-based molecular junctions are facing: the relatively low connection yield (~3–5%) and the variation of the device-to-device properties resulting from the variability in the properties of SWNTs that depend on their chirality and diameter. In conjunction with the unique properties of graphene electrodes, the ease of device fabrication and the device stability place graphene–molecule junctions as a new-generation testbed for molecular electronics. It should be mentioned that nanoscale SWNT and graphene electrodes can also be made by electric breakdown.[24,25]

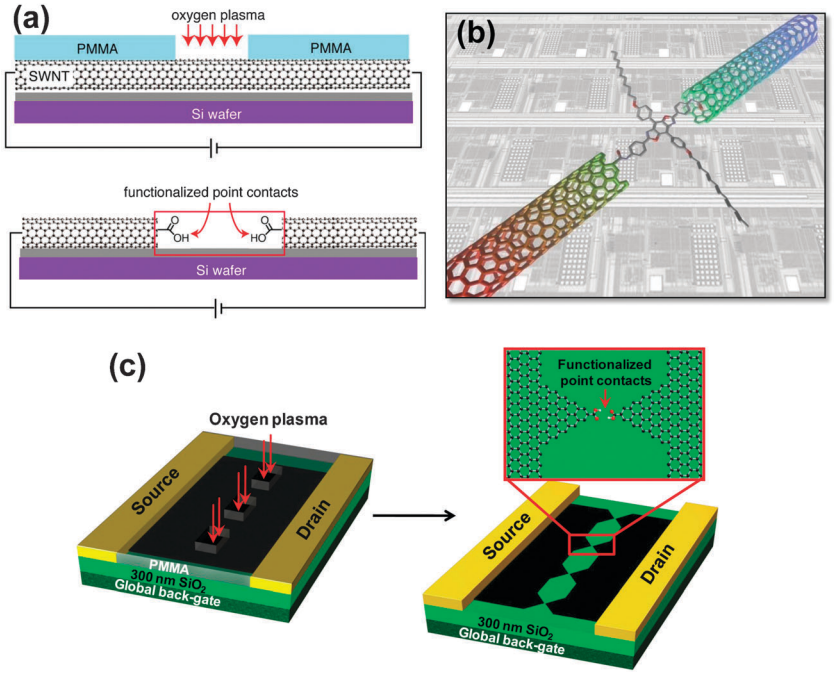

Fig. 7 (a) Schematic representation of cutting SWNTs as carboxylic acid-functionalized point contacts. Reproduced with permission from ref. 22. Copyright 2006 American Association for the Advancement of Science. (b) The corresponding single-molecule junctions. Reproduced with permission from ref. 4. Copyright 2008 American Chemical Society. (c) Schematic representation of building single-molecule junctions using point contacts made from graphene as electrodes through a DLL process. Reproduced with permission from ref. 23. Copyright 2012 Wiley-VCH Verlag GmbH & Co. KGaA.

In these cases, molecules with terminal groups of aromatic rings, such as phenanthrene and anthracene, can bridge the electrodes through π–π stacking interactions.

Besides metal and carbon-based electrodes, some other novel electrodes, such as silicon and conductive polymers, have also been developed to realize the controllable fabrication and interfacial regulation of molecular junctions. Silicon, due to its controllable conductivity, tunable Fermi level by doping, mature processing technology, and well-established covalent grafting methods with molecules, has the obvious advantages to be fabricated as electrodes for molecular junctions. Ashwell *et al.*[26] used highly doped n-type Si(111) as a lower electrode and polycrystalline Si as an upper electrode to prepare molecular junctions with a sandwich structure (Fig. 8a). 4-Ethynylbenzaldehyde, which is used as a molecular bridge to connect targeted molecules to amino-terminated units to Si electrodes, is first covalently grafted to Si electrodes through a simple thermally-activated addition reaction. Importantly, the robust Si–C covalent bond connection is constructed at the molecule–electrode interface of molecular junctions. In another case, single conductive polymers were used as electrodes in molecular junctions, which is able to reduce the electrode width down to the molecular level and might be helpful for the fabrication of future practical single-molecule integrated circuits. Through chemical wiring and soldering methods, Okawa *et al.*[27] have fabricated an all-molecule electronic circuit with conjugated polymer nanowires (Fig. 8b). Conductive polydiacetylene (PDA) nanowire electrodes were created by pulsed bias voltages, which stimulate the chain polymerization of self-assembled monolayer (SAM) diacetylene compounds at designated positions, from the tip of a scanning tunneling microscope (STM). When the PDA chain reached the absorbed functional phthalocyanine molecule, the reactive carbene end of PDA was then inserted into a C–H bond of phthalocyanine. This carbene C–H insertion forms a covalent sp^3 carbon atom connection at the contact point, which is expected to be a potential energy barrier for the electrons flowing. Due to the existence of the energy barrier at the molecule–electrode interface, such single-molecule junctions may have interesting performance as a resonant-tunneling diode.

4.2 Different anchoring groups

The anchoring groups of the molecules used for building molecule–electrode contacts are another important parameter for the interfacial control of molecular junctions, which help to determine the molecule–electrode binding strength and the energy levels of the frontier molecular orbitals for charge transport. The abundant species of anchoring groups make it convenient to control the interfacial characteristics of molecular junctions by properly selecting the anchoring groups at the molecular ends. Due to the intrinsic advantages of gold electrodes, the majority of the investigations of the anchoring group effects on the properties of molecular junctions were carried out in gold electrode systems. Here, we summarize the effects of the anchoring groups used in gold electrode-based molecular junctions on the interfacial properties (Table 1).

For gold electrodes, thiol groups (–SH) are widely used for the connection between the molecules and the electrodes

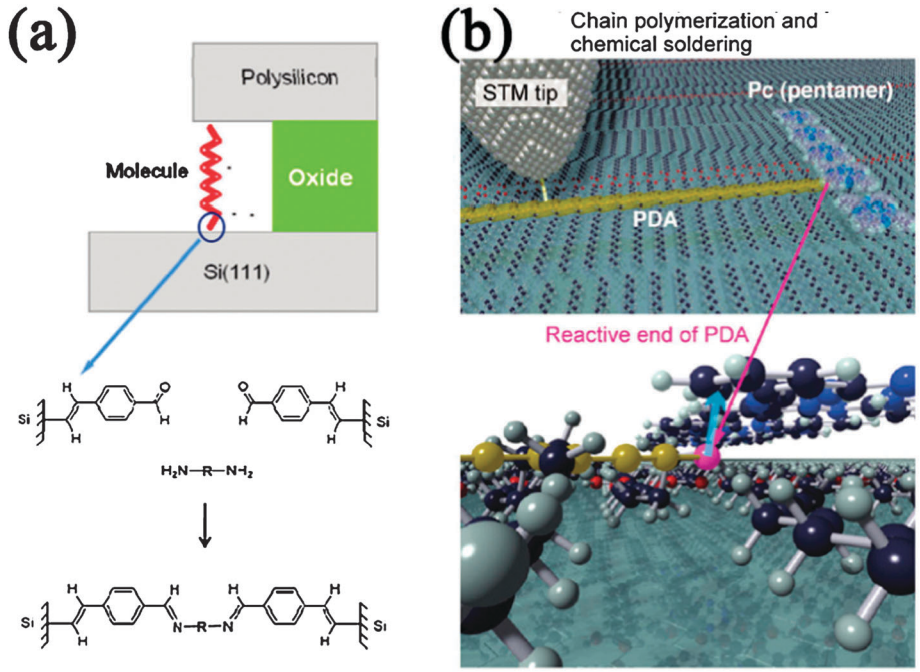

Fig. 8 (a) Schematic representation of silicon electrode-based molecular junctions with 4-ethynylbenzaldehyde as molecular bridges. Reproduced with permission from ref. 26. Copyright 2010 American Chemical Society. (b) Schematic representation of PDA nanowire electrodes connected to the phthalocyanine molecule. Reproduced with permission from ref. 27. Copyright 2011 American Chemical Society.

because of the high covalent strength and good electronic coupling of the formed Au–S covalent bond. However, due to the large variability in Au–S binding geometries, multiple and broadened conductance distribution are usually observed for thiol-terminated molecular junctions.[13] In addition, dithiols are easy to polymerize because of the oxidative disulfide formation. The other early-developed anchoring groups, such as isocyanide (–N≡C),[30] selenium and carboxylic acid (–COOH),[28] also suffer the similar complications as thiols, and the coupling of –N≡C or –COOH with gold electrodes is not as good as that of –SH.

Interestingly, for amine ($-NH_2$) anchoring groups,[41] the N lone electron pair of amines preferentially binds to coordinatively unsaturated surface Au atoms with the formation of an Au–N D–A bond. Though such an Au–N D–A bond is weaker than an Au–S covalent bond, it is insensitive to the local structure of the bonding points and provides well-defined electronic coupling at Au–N contacts. Therefore, repeatable interfacial contacts and single narrow distributional conductance can be realized for diamine molecule–Au junctions. Based on the similar principle of coordination chemistry, a series of different anchoring groups were developed to accomplish the well-defined interfacial control by forming different D–A bonds, such as amine ($-NH_2$),[41] pyridine[33] and nitrile (–C≡N)[34] terminal groups for Au–N D–A bonds, methyl sulfide (–SMe)[31] and isothiocyanate (–NCS)[18] terminal group for Au–S D–A bonds, dimethylphosphine ($-PMe_2$)[31] and diphenylphosphine ($-PPh_2$)[35] for Au–P D–A bonds.

By comparing Au–N, Au–S, and Au–P D–A bonds, it was found that the binding strength and conductivity gradually increased from Au–NH_2R and Au–SMeR to Au–PMe_2R.[31] For a single σ-donation from the lone electron pair to the Au atom, the phosphines are the strongest, followed by the amines, and the sulfides are the weakest. However, the increased availability of ligand d states in sulfides and phosphines leads to π-back-donation from the Au atom to the ligands, which is the strongest for the phosphines, then for the sulfides, and the weakest for amines. This π-back-donation provides an additional channel for electron transport, leading to a decrease in the contact resistance. Therefore, the balance of these processes results in the increasing trend in the electronic coupling strength from Au–N, Au–S to Au–P.

For Au–N D–A bonds, different anchoring groups can be used to adjust the energy levels of the frontier molecular orbitals for charge transport. Electron-donating amine groups[41] lift the frontier orbital energies and bring the HOMO of molecules closer to the Fermi level, which favors hole transport. In contrast, electron-withdrawing pyridine[33] and nitrile (–C≡N)[34] groups decrease the frontier orbital energies and promote electron transport by reducing the energy offset between the LUMO of molecules and the Fermi level of electrodes. In addition to the energy levels, we notice that the molecule–electrode coupling strength also has certain differences for different Au–N bond systems.[12] The Au–N bond of pyridine is stronger than that of amine. This is because the π-space of pyridine contributes to the binding although an sp^2-derived lone pair of pyridine is less sharply directed in space than an sp^3 derived lone pair of amine. However, for amine anchoring groups alone, when the amine group is connected to the aromatic ring, such as 1,4-benzenediamine,

Table 1 List of anchoring groups and related characteristics in Au–molecule–Au junctions[a]

Anchoring groups	Molecules	Conductance/G_0	Binding energy/eV	Ref.
–SH	$HS(CH_2)_nSH$	G_{con} = 0.60 (HC), β_N = 1.01 G_{con} = 0.10 (LC), β_N = 0.98	1.7 (TH) 1.2 (AT)	18, 28
	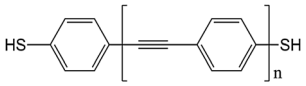	$G_{n=0}$ = 8.3 × 10^{-3}, β = 0.32		29
–N≡C	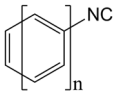	G_{con} = 0.0036, β = 0.49 (G_{-SH} = 0.001)		30
–COOH	$HOOC(CH_2)_nCOOH$	G_{con} = 0.007 (HC), β_N = 0.81 G_{con} = 0.0006 (LC), β_N = 0.77	0.17	28
$-NH_2$	$H_2N(CH_2)_nNH_2$	G_{con} = 0.035, β_N = 0.93	0.7	31
Pyridine	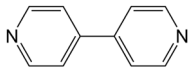	G = 1 × 10^{-3} (HC), G = 3 × 10^{-4} (LC)	1.36	32, 33
–C≡N	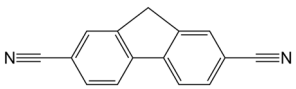	G = 9.2 × 10^{-5}	1.05	34
SMe	$MeS(CH_2)_nSMe$	G_{con} = 0.048, β_N = 0.89	0.6	31
–NCS	$NCS(CH_2)_nSCN$	G_{con} = 0.10 (HC), β_N = 1.01 G_{con} = 0.008 (LC), β_N = 0.96	0.8 (TH) 1.1 (AT)	18
$-PMe_2$	$Me_2P(CH_2)_nPMe_2$	G_{con} = 0.10, β_N = 1.02	1.2	31
$-PPh_2$	$Ph_2P(CH_2)_nPPh_2$	G_{con} = 0.072, β_N = 0.98	1.0	35
$-CS_2H$	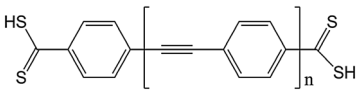	$G_{n=0}$ = 4.8 × 10^{-3}, β = 0.05		29
$-NCS_2H$	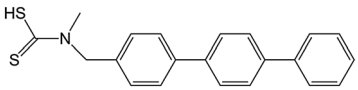	J = 1.13 × 10^{-3} (A cm^{-2}) (J_{-SH} = 1.39 × 10^{-5} (A cm^{-2}))	1.5	36
$-SnMe_3$	$Me_3Sn(CH_2)_nSnMe_3$	$G_{n=4}$ = 0.09, β_N = 0.97 (G_{-NH_2} = 9 × 10^{-4})	3.0	37
	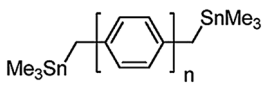	$G_{n=1}$ = 0.9, β = 0.43		38
$-C_{60}$	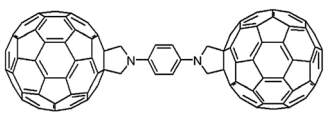	G = 3 × 10^{-4} (G_{-NH_2} = 4 × 10^{-4})	0.67	39, 40
Strained benzene	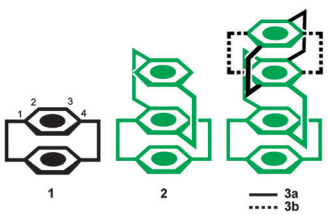	$G_{n=1}$ = 0.01, β = 0.63	0.74	40

[a] The conductance with the change in molecular length is $G = G_{con}e^{-\beta d}$, where G_{con} is the contact conductance, β the decay constant and d the width of the tunneling barrier.[1] β_N and β in Table 1 denote the decay constant per $-CH_2$ unit and Angstrom, respectively. Using a C–C vertical separation of 1.27 Å,[37] the relationship between β_N and β is $\beta_N = 1.27\beta$. HC is the conductance for the high conductance state, and LC is the conductance for the low conductance state. The conductance in the parentheses is the compared conductance for the similar system with changed terminal groups. All the contact resistances mentioned in some literature are converted into contact conductances ($G_0 = 2e^2/h$ = 77.5 μS = 12.9 kΩ). Some binding energies are calculated from the desorption energy of the molecules (1 eV per atom = 96.485 kJ mol^{-1} = 23.06 kcal mol^{-1}).[28,36] TH is the binding energy at the three-fold hollow site and AT is the binding energy at the atop site.

the Au–N D–A bond is weakened because the N lone pair is partly delocalized into the molecular π-system.

For Au–S D–A bonds, the –NCS headgroup, which is an electron-rich ligand with π-conjugation, can strongly bind to the Au electrodes with π orbital contribution, but exhibits low conductance values (see the discussion in the above section).[18] For Au–P D–A bonds, $–PMe_2$ and $–PPh_2$ anchoring groups were developed to realize the strong binding between the terminal groups and the gold electrodes.[35] However, due to the high reactivity of $–PMe_2$, the PMe_2-terminated molecules are reactively unstable in the ambient environment. Fortunately, the $–PPh_2$ anchoring groups can link to the gold electrodes with similar coupling conditions to the $–PMe_2$ groups, but are air-stable.

As discussed above, one important goal of anchoring group selections is to enhance the coupling strength between the molecules and the electrodes and then reduce the contact resistance for satisfying the measurement of intrinsic charge transport in molecular junctions. An improved way to realize this is to increase the electron delocalization of terminal groups and the number of coupling electronic channels at the contacts. The carbodithioate ($–CS_2H$) group,[29] which has two terminal sulfurs and the delocalized electronic structure with π conjugation, proves to be a good candidate because it can couple with Au electrodes through double-bonded sulfurs. Due to the s and p states of carbodithioate groups (CS_2), they can hybridize with d states of gold and create an additional π-mediated coupling pathway for charge transport. Therefore, the enhanced electronic coupling and reduced charge transport barrier afford a much larger conductivity of carbodithioate-bridged molecular junctions than that of classic thiol-linked molecular junctions. Another interesting anchoring group, dithiocarbamate ($–NCS_2H$), was chosen by Wrochem *et al.*[36] to build superior electrical contacts for molecular junctions. Similar to the carbodithioate group, the s and p states on the CS_2 moiety of dithiocarbamate (NCS_2) could hybridize with the d states of gold. In addition, the nonbonding electron pair on the N atom could enhance the strength and delocalization of S–Au antibonding states resulting from the hybridization of thiolate frontier orbitals (sulphur 3p states) with gold d and s states. Due to the electron donating effect of the nitrogen lone pair, the energy offset between the HOMO and the Fermi level is also reduced. Therefore, the proved delocalized electronic states of dithiocarbamate anchoring groups linked to gold result in a significant drop in the contact resistance by about two orders of magnitude compared to thiolates on gold and the high stability of dithiocarbamate-linked molecular junctions.

Another efficient way to realize the strong interfacial coupling and high conductivity of MTJs is to covalently bond the carbon backbone of the molecules to the electrodes without intervening groups. Cheng *et al.*[37] used trimethyl tin ($SnMe_3$)-terminated molecules to form *in situ* covalent Au–C σ bond connections by directly displacing the $SnMe_3$ linkers at the molecular ends with gold atoms. Due to the high coupling of Au–C σ bond orbitals, the conductance of direct Au–C bonded alkanes is ~100 times larger than those of analogous alkanes with most other terminal groups. However, for π-conjugated molecules, such as benzene, when Au atoms are directly bonded to the sp^2 benzene carbon, the benzene π system is not well coupled with the σ channel of Au–C bonds and thus the conductance is not very high for Au–C bonded benzene molecular junctions. In contrast, when the conjugated system has a terminal methylene group at each end, the strong electronic coupling between the electrodes and the molecular π system can be achieved for Au–C bonded molecular junctions.[38] For instance, Au–C bonds of xylylene are well coupled with the π system, and a conductance approaching one quantum conductance ($G_0 = 2e^2/h$) is obtained for Au–C bonded *p*-xylylene molecular junctions.

In some cases, when the terminals of molecules have strained aromatic rings, the direct metal–carbon coupling can also be realized. For example, fullerene (C_{60}) has been developed as an anchoring group for molecular junctions.[39] As anchoring groups, C_{60} moieties can strongly be adsorbed on gold surfaces *via* a hexagonal ring or a [6,6] double bond through partial charge transfer and strong hybridization between C_{60} and surface gold atoms. Due to the size and symmetry of C_{60} molecules, the conductance of C_{60}-linked molecular junctions is insensitive to the details of the contact geometries. In addition, due to the large size of C_{60} terminal groups, the molecule can be directly visualized and individually targeted to gold electrodes using a scanning tunneling microscope (STM), thus ensuring the formation of unambiguous single-molecule junctions.[42] In another case, for multiple π–π stacked aromatic rings,[40] which are held together *via* a paracyclophane scaffold, gold atoms can directly bind to two neighboring carbon atoms of the outermost cyclophane benzene rings in an η^2-fashion. The strained structure of the outmost benzene rings is necessary for the bonding, and the electron-donating substituent could strengthen the bonding. With direct Au–C bonds, Au electrodes can couple with the molecular π system, which facilitates charge transport through the π system.

4.3 Molecular environments

External environments and conditions, such as mechanical forces and molecular environments, can influence the contact interfacial characteristics of molecular junctions. For example, it was found that mechanical forces can adjust the electrode–molecule contact geometry and thus the coupling strength. In pyridine–gold single-molecule junctions, reversible switching properties between two conductance states, which is due to distinct contact geometries at nitrogen–gold bonds (Fig. 9a), were realized through junction elongation and compression.[32,33] During the contact formation, the nitrogen lone pairs in pyridine are donated to the partially-empty s-orbital of gold atoms to form nitrogen–gold bonds along the molecule backbone. When the junction is elongated, the essential transmission channel, LUMO π*-orbital, is expected orthogonal to the nitrogen lone pair, which leads to the low electronic coupling and the low conductance. In contrast, during junction compression,

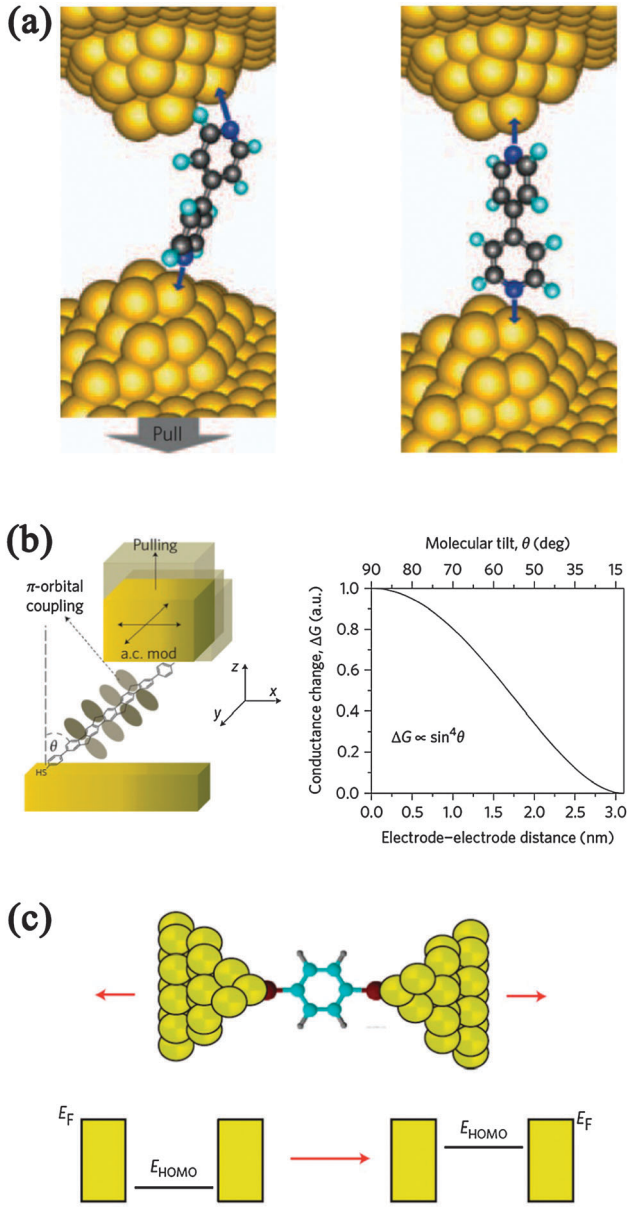

Fig. 9 (a) Schematics illustrating mechanically-induced configuration changes for pyridine–gold molecular junction. Reproduced with permission from ref. 32. Copyright 2009 Nature Publishing Group. (b) Schematic of lateral coupling experiments (left) and the conductance change *versus* electrode–electrode distance and tilt angle θ (right). Reproduced with permission from ref. 43. Copyright 2011 Nature Publishing Group. (c) Schematic of a BDT molecular junction and the energy change in the HOMO relative to E_F with the increased electrode separation. Reproduced with permission from ref. 44. Copyright 2012 Nature Publishing Group.

the contact gold atom and bond may shift from one site of the electrode to another with nitrogen–gold bonds tilted out of the plane of the π*-system. A significant overlap between the LUMO and the orbitals of adjacent gold contact atoms may occur. This extra lateral electronic coupling enhancement could result in the high conductance state of single-molecule junctions. More accurate mechanical control of the lateral coupling of single-molecule junctions was performed by Diez-Perez *et al.*[43] In this work, a pentaphenylene molecule, which has highly delocalized π-molecular orbitals, a large band gap enough for non-resonant tunneling, and long alkyl side chains for avoiding intermolecular π–π stacking, was fixed into the gap of two gold electrodes with Au–S covalent bonds. Through gradual mechanically-adjusted electrode separation (Fig. 9b), the tilt angle θ between the π-conjugated molecular backbone and the surface of two electrodes can be continuously fine-tuned. They found that with the increase in the tilt angle, the lateral coupling between the π orbitals of the molecule and the orbitals of Au electrodes was enhanced. This enhanced lateral coupling led to a monotonic increase in molecular conductance, which perfectly fits the theoretical prediction that $G \propto \sin^4\theta$. In addition, mechanical forces can also modulate the molecular orbital alignment. Using 1,4-benzenedithiol (BDT) as a model molecule, Bruot *et al.*[44] investigated the electromechanical properties of molecular junctions. With gradual stretching of the junction at the contacts (Fig. 9c), the electronic coupling between the molecules and the electrodes was weakened. This causes a shift of the HOMO level closer to the Fermi level of the electrodes, thus leading to a resonant enhancement of the conductance.

As mentioned above, external molecular environments have an effect on the contact interfacial features of molecular junctions. This is majorly through directly affecting the contact points or the electrode atoms adjacent to the contact points. By using gold–thiol molecular junctions, Long *et al.*[45] found that hydration at Au–S contacts greatly affects molecular conductance (Fig. 10a, left). When molecular junctions were exposed to the environment with water vapors, protons resulting from water could strongly interact with the lone pair electrons of sulphur atoms at the contact with the formation of weakened S–H bonds, as evidenced by a certain red-shift of the peaks compared to free thiols from IETS studies (Fig. 10a, right). Due to the formation of S–H bonds, the strong Au–S coupling at the electrode–molecule contact is weakened, which suppresses the electronic coupling between the molecules and the electrodes and thus led to the decrease in conductance of molecular junctions. In general, the reactivity between the sulphur atoms and the water is higher in alkyl junctions than that in aromatic junctions due to the stronger electron–donor ability induced by the alkyl *versus* the aromatic moieties. However, because of the resonance stabilization of the aromatic ring system, the strength of the S–H bonds formed is stronger for aromatic junctions than that for alkyl junctions.

It was also found that external molecular environments could adjust the energy level alignment between the electrode Fermi level and the molecular orbitals as demonstrated by Fatemi *et al.*[46] Using 1,4-benzenediamine (BDA)–Au molecular junctions, they studied the effects of different solvent environments on the conductance of molecular junctions. At the contact of BDA–Au molecular junctions, the Au–N D–A bond formed induces partial charge transfer from the molecule to the electrode surface, which generates a surface-induced dipole at the interfaces (Fig. 10b, right). This surface-induced dipole decreases the work function of Au electrodes, thus increasing the energy level difference (ΔE_{HOMO}) between the Fermi level of electrodes and the HOMO of molecules. As HOMO is the main

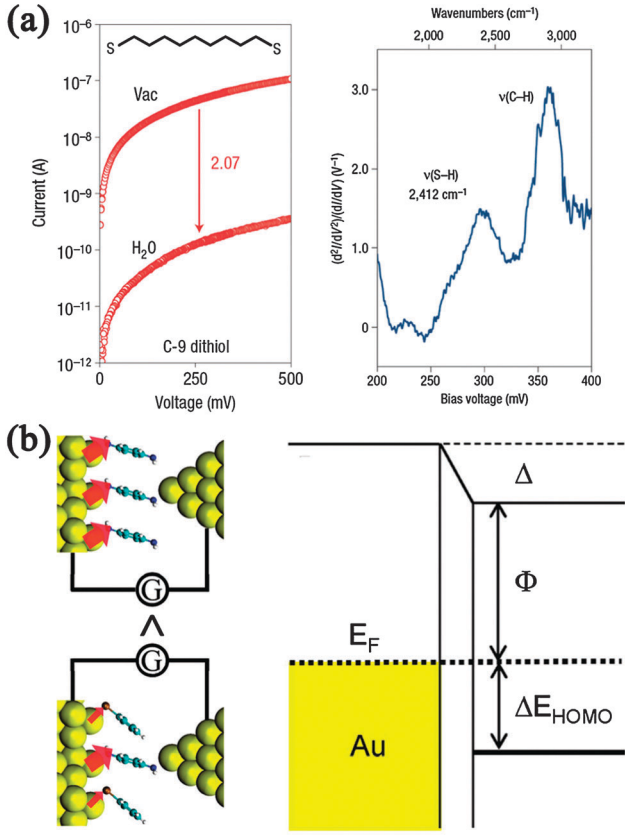

Fig. 10 (a) *I–V* characteristics of a C-9 alkanethiol junction under anhydrous and hydrated conditions (left). IETS analysis of a hydrated C-9 junction showing a prominent red-shifted S–H stretching vibration (right). Reproduced with permission from ref. 45. Copyright 2006 Nature Publishing Group. (b) Schematics illustrating the adjacent adsorbed BDA molecules around BDA molecular junctions replaced by solvent molecules (left) and the energy band structure change with a surface dipole induced level shift Δ (right). Reproduced with permission from ref. 46. Copyright 2011 American Chemical Society.

transmission channel for BDA junctions, ΔE_{HOMO} plays an important role in the junction conductance. When the adjacent adsorbed BDA molecules at undercoordinated binding sites on the Au surface were replaced by electron-withdrawing solvent molecules (Fig. 10b, left), such as chlorobenzene (ClPh), bromobenzene (BrPh) and iodobenzene (IPh), the electrode work function is increased and then the related surface-induced dipole at Au–N contacts is reduced. Therefore, the adsorption of solvent molecules leads to the reduction of ΔE_{HOMO} and the corresponding increase of the junction conductance. Interestingly, this effect shows the solvent dependence. With the increased binding energies from ClPh to IPh, the effect is enhanced because the replacement probability and local coverage of solvent molecules increased. Note that due to the high binding energy and replacement probability of IPh, lower forming probability and stability of BDA junctions were observed in IPh solvent.

4.4 Intramolecular connections

All the discussions mentioned above are the strategies developed for controlling the interfacial properties by adjusting the electronic coupling between the molecules and the electrodes (the intermolecular coupling). In addition to the intermolecular coupling, the intramolecular coupling, which happens between the anchoring groups and the main backbone of the same molecules, proves to be an alternative strategy for controlling the interfacial properties by precisely designing the chemical structures of molecules. Normally, saturated carbon atom connections are used for the weak intramolecular coupling, which is utilized in some functional molecular junctions[47] requiring robust contacts and weak coupling between the electrodes and the molecules. In contrast, direct π-conjugated bonds are used for the strong intramolecular coupling, which is usually needed for intramolecular energy self-matching between molecular terminal groups and the molecular backbone.[37] In addition, bridge molecules,[26] which are first anchored on each side of the electrodes and then connected to targeted molecules, can also be used as intramolecular connections to adjust the electronic coupling between the anchoring groups and the main molecules.

5. Effects of the molecule–electrode interfaces on device functionalities

As discussed above, proper selections of electrode materials, anchoring groups, intramolecular connections and external environments prove to be an efficient approach for precisely

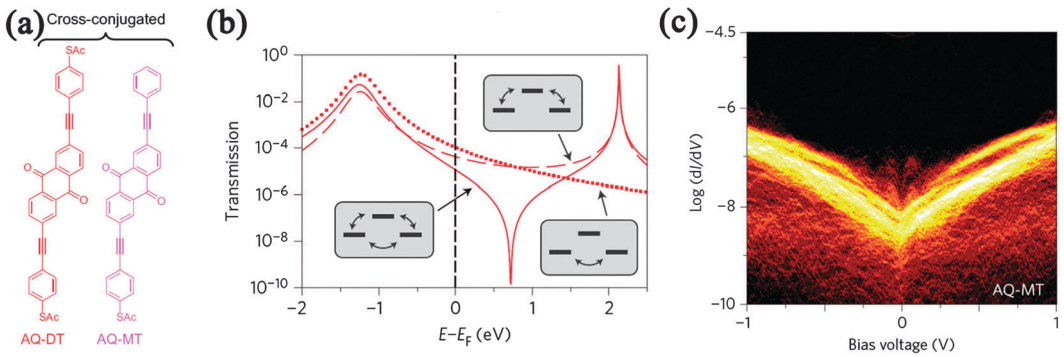

Fig. 11 (a) Molecular structures used for quantum interference investigations. (b) Schematics illustrating the origin of interference in cross-conjugated molecules. (c) Two-dimensional conductance histogram of AQ–MT molecular junctions. Reproduced with permission from ref. 48. Copyright 2012 Nature Publishing Group.

controlling the contact characteristics of molecule–electrode interfaces, such as the bonding type, the coupling strength and the energy level alignment. Eventually, precise interface control is helpful to better understand charge transport mechanisms of molecular junctions and then realize the regulation of their electrical properties, which should provide new insights into designing new types of reliable molecular electronic devices with novel functionalities.

5.1 Novel quantum effects

As discussed in the second section, quantum transport properties of molecular junctions are intimately related to the nature of the molecule–electrode interface, such as Coulomb blockade induced by the weak coupling, Kondo resonance and co-tunneling by the intermediate coupling, and high quantum conductance by the strong coupling. Without doubt, novel interface-induced quantum effects can be observed in MTJs through precise interface modulations. Theorists have predicted that it should be possible to observe quantum interference in molecular junctions through direct manipulation of the electron wavefunctions. Indeed, recently Guédon *et al.*[48] reported the observation of destructive quantum interference in charge transport through proper selections of the endgroups and the molecular backbones at room temperature, using two-terminal molecular junctions. They found that for molecules with a cross-conjugated anthraquinone unit and phenylene–ethynylene endgroups (Fig. 11a), the electron waves propagate through two distinct paths: HOMO and LUMO, which have a phase difference of π. The theoretical calculation of the energy-dependent transmission function, which describes the quantum-mechanical probability that an electron with energy E traverses the molecular junction, shows that when the partial waves have equal weight at a proper energy, an interference minimum ('anti-resonance') can be observed (Fig. 11b). Consistently, when the Fermi level (E_F) is experimentally adjusted lying near the interference minimum with one gold–sulphur dipole, a zero-bias anomaly was observed (Fig. 11c), which is the direct proof of destructive quantum interference for charge transport through molecular junctions.

5.2 Novel functionalities

Since molecule–electrode interface engineering can efficiently control the coupling strength and improve the molecular conductance, it should also be a powerful approach for installing novel functionalities in molecular junctions. For example, in molecular junctions formed from redox-active molecules, conductance switching can be realized by adjusting the redox states of functional groups through electrochemical gating or chemical treatments. To do this, it would be better to connect functional groups to electrodes through saturated carbon atoms for the purpose of reducing the electronic coupling between redox-active units and electrodes and thus preventing charge transfer between them, as demonstrated by Liao *et al.* (Fig. 12a).[47] In this work, when molecular junctions are treated with the oxidizing agent, such as iron chloride, the TTF unit is oxidized to form its oxidation state with a rearrangement of the TTF molecular orbitals, which leads to an order of magnitude increase of the conductance. When treated with the

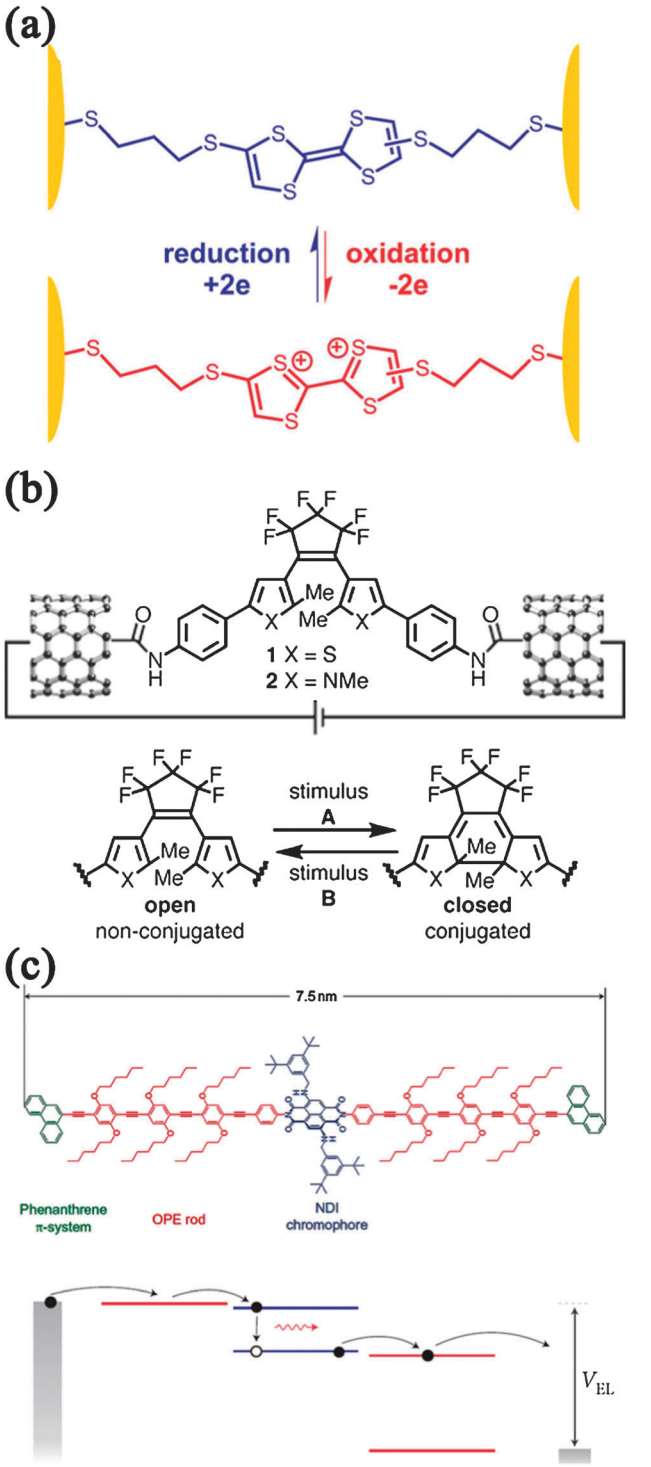

Fig. 12 (a) Chemical structure of dithiolated tetrathiafulvalene derivatives used for redox-active molecular junctions. Reproduced with permission from ref. 47. Copyright 2010 American Chemical Society. (b) Diarylethenes connected to nanogapped SWNT electrodes through amide linkages. Reproduced with permission from ref. 50. Copyright 2007 American Chemical Society. (c) Chemical structure of molecules and the energy-level model for electroluminescence. Reproduced with permission from ref. 24. Copyright 2010 Nature Publishing Group.

reducing agent, such as ferrocene, the oxidized TTF unit is reduced to its original neutral state. Correspondingly, the conductance switches back.

For another example, when individual diarylethene, a typical photochromic molecule which can undergo reversible transitions between two distinct isomers with open–closed conformations, was wired into gold electrodes through Au–S D–A bonds, the device showed a novel photoswitching effect but only from the closed form to the open form. This should be ascribed to the quenching effect of the photoexcited open form by the Fermi level of gold electrodes and thus the inhibition of the closing reaction.[49] In another case, when diarylethene molecules were immobilized inside the gaps of SWNT point contacts through covalent amide linkages,[50] the devices also showed similar photoswitching properties but only from the open state to the closed state (Fig. 12b). This is attributed to the energy transfer of the photoexcited closed state to the extended π-electron system, *i.e.* SWNTs. Remarkably, this result is exactly the opposite of the work done on gold electrodes as discussed above, which strongly stresses the crucial importance of the extent of molecule–electrode coupling to the device performance.

With proper interfacial coupling and good energy level alignment, electroluminescence from single-molecule junctions can be realized in the system where fluorescent chromophores are used as functional units. For instance, Marquardt *et al.*[24] have observed electroluminescence in a single nanotube–molecule–nanotube junction formed from a molecule that has a naphthalenediimide (NDI) dye with the strong fluorescence signal as the functional center and two long oligo(phenylene ethynylene) (OPE) rods as the anchoring groups (Fig. 12c). Through π–π interactions, individual molecules were electrostatically trapped into the gaps of SWNTs. Such π–π connection led to intermediate coupling between the molecules and the electrodes, which is important in favoring the co-tunneling process of charge transport, thus leaving the molecules in the excited state for luminous emission. In addition, due to almost perpendicular torsion angles at the imide positions between NDI and OPE rods, π conjugation between functional units and anchoring groups are interrupted, resulting in the weak intramolecular coupling. Therefore, the voltage drops are assumed mainly at the weak imide links between NDI and OPE rods. With the applied potential increased to a certain degree, the energies of the two orbitals of NDI overlapping with the OPE rods have to be located between the energy of the HOMO to the left and the LUMO to the right OPE wire (Fig. 12c). Electrons and holes are then simultaneously injected into the NDI chromophore, where they recombine with light emission.

6. Conclusion and perspective

In this article, we highlighted the significant effect of the molecule–electrode interfaces on the electrical properties of molecular junctions. Through proper selections of electrode materials, anchoring groups, intramolecular connections, and external environments, discrete approaches have been developed to precisely control the interfacial properties of the molecule–electrode interfaces, such as the bonding type, the coupling strength and the energy level alignment. Therefore, molecule–electrode interface engineering proves to be an efficient and powerful approach for controlling the interfacial electronic structure, improving the molecular conductance, and even installing novel functionalities in molecular junctions. The analyses demonstrated in this review should be valuable for deeply understanding the relationship between the contact interface and the charge transport mechanism, which is of crucial importance for the development of reliable molecular electronic devices with desired functionalities in future.

Despite significant progresses achieved over the past decade, molecular electronics is still in its infancy. One of the major challenges primarily stems from the device-to-device heterogeneity in their baseline electronic properties. This is because of the lack of precise control of the fabrication process, the contact geometry, the molecular conformation, the exact number of molecules to be tested, and the measurement condition. Therefore, to fabricate reliable molecular devices, one should try as best as possible to consider all the parameters as a holistic one. The electrode materials, molecular materials, the contact interfaces, the device fabrications, and the experimental environments, *etc.* are so closely interrelated that they cannot be optimized independently. Consequently, developing a reliable and scalable fabrication methodology for mass-producing identical MTJ arrays in high yields by holistic consideration of all these parameters is currently one of the central research focuses. We expect that the combination of materials fabrication and interface engineering with flexible molecular design could speed the development of molecular electronics. Another formidable issue in molecular electronics is a great shortage of efficient integration strategies. Predictably, the next generation of devices would be a network of interface where the molecules function as pivotal elements to control the interface. In addition, although several useful analytic techniques (such as IETS, TVS, thermoelectricity and force measurements) have been developed for characterizing the electrode–molecule interface, those methods are indirect and incomplete. Developing new efficient techniques for directly extracting more details from molecular junctions is highly desirable at present.

This review exemplifies the current interests and efforts in making functional molecular devices through interface engineering. We can expect that molecular electronics, as required by the diverse expertise critical to making key advances in the field, will foster truly excellent collaboration bringing materials, chemistry and physics together, thus forcing the rapid development of the field.

Acknowledgements

We acknowledge primary financial support from MOST (2012CB921404) and NSFC (21225311, 51121091, and 2112016).

References

1 S. Karthauser, *J. Phys.: Condens. Matter*, 2011, **23**, 013001.
2 T. Li, W. P. Hu and D. B. Zhu, *Adv. Mater.*, 2010, **22**, 286.
3 H. Song, M. A. Reed and T. Lee, *Adv. Mater.*, 2011, **23**, 1583.
4 A. K. Feldman, M. L. Steigerwald, X. F. Guo and C. Nuckolls, *Acc. Chem. Res.*, 2008, **41**, 1731.
5 K. Moth-Poulsen and T. Bjornholm, *Nat. Nanotechnol.*, 2009, **4**, 551.
6 L. Bogani and W. Wernsdorfer, *Nat. Mater.*, 2008, **7**, 179.
7 M. A. Reed, *Mater. Today*, 2008, **11**, 46.
8 Y. Kim, T. J. Hellmuth, M. Burkle, F. Pauly and E. Scheer, *ACS Nano*, 2011, **5**, 4104.
9 M. Araidai and M. Tsukada, *Phys. Rev. B: Condens. Matter Mater. Phys.*, 2010, **81**, 235114.
10 P. Reddy, S. Y. Jang, R. A. Segalman and A. Majumdar, *Science*, 2007, **315**, 1568.
11 J. R. Widawsky, P. Darancet, J. B. Neaton and L. Venkataraman, *Nano Lett.*, 2012, **12**, 354.
12 M. Frei, S. V. Aradhya, M. Koentopp, M. S. Hybertsen and L. Venkataraman, *Nano Lett.*, 2011, **11**, 1518.
13 M. Frei, S. V. Aradhya, M. S. Hybertsen and L. Venkataraman, *J. Am. Chem. Soc.*, 2012, **134**, 4003.
14 M. Tsutsui, M. Taniguchi and T. Kawai, *J. Am. Chem. Soc.*, 2009, **131**, 10552.
15 Z. F. Huang, F. Chen, R. D'Agosta, P. A. Bennett, M. Di Ventra and N. J. Tao, *Nat. Nanotechnol.*, 2007, **2**, 698.
16 J. M. Beebe, B. Kim, C. D. Frisbie and J. G. Kushmerick, *ACS Nano*, 2008, **2**, 827.
17 A. P. Bonifas and R. L. McCreery, *Nat. Nanotechnol.*, 2010, **5**, 612.
18 C. H. Ko, M. J. Huang, M. D. Fu and C. H. Chen, *J. Am. Chem. Soc.*, 2010, **132**, 756.
19 A. Sen and C. C. Kaun, *ACS Nano*, 2010, **4**, 6404.
20 H. J. Yan, A. J. Bergren and R. L. McCreery, *J. Am. Chem. Soc.*, 2011, **133**, 19168.
21 T. Li, J. R. Hauptmann, Z. M. Wei, S. Petersen, N. Bovet, T. Vosch, J. Nygard, W. P. Hu, Y. Q. Liu, T. Bjornholm, K. Norgaard and B. W. Laursen, *Adv. Mater.*, 2012, **24**, 1333.
22 X. F. Guo, J. P. Small, J. E. Klare, Y. L. Wang, M. S. Purewal, I. W. Tam, B. H. Hong, R. Caldwell, L. M. Huang, S. O'Brien, J. M. Yan, R. Breslow, S. J. Wind, J. Hone, P. Kim and C. Nuckolls, *Science*, 2006, **311**, 356.
23 Y. Cao, S. H. Dong, S. Liu, L. He, L. Gan, X. M. Yu, M. L. Steigerwald, X. S. Wu, Z. F. Liu and X. F. Guo, *Angew. Chem., Int. Ed.*, 2012, **124**, 12394.
24 C. W. Marquardt, S. Grunder, A. Blaszczyk, S. Dehm, F. Hennrich, H. von Lohneysen, M. Mayor and R. Krupke, *Nat. Nanotechnol.*, 2010, **5**, 863.
25 F. Prins, A. Barreiro, J. W. Ruitenberg, J. S. Seldenthuis, N. Aliaga-Alcalde, L. M. K. Vandersypen and H. S. J. van der Zant, *Nano Lett.*, 2011, **11**, 4607.
26 G. J. Ashwell, L. J. Phillips, B. J. Robinson, B. Urasinska-Wojcik, C. J. Lambert, I. M. Grace, M. R. Bryce, R. Jitchati, M. Tavasli, T. I. Cox, I. C. Sage, R. P. Tuffin and S. Ray, *ACS Nano*, 2010, **4**, 7401.
27 Y. Okawa, S. K. Mandal, C. P. Hu, Y. Tateyama, S. Goedecker, S. Tsukamoto, T. Hasegawa, J. K. Gimzewski and M. Aono, *J. Am. Chem. Soc.*, 2011, **133**, 8227.
28 F. Chen, X. L. Li, J. Hihath, Z. F. Huang and N. J. Tao, *J. Am. Chem. Soc.*, 2006, **128**, 15874.
29 Y. J. Xing, T. H. Park, R. Venkatramani, S. Keinan, D. N. Beratan, M. J. Therien and E. Borguet, *J. Am. Chem. Soc.*, 2010, **132**, 7946.
30 B. Kim, J. M. Beebe, Y. Jun, X. Y. Zhu and C. D. Frisbie, *J. Am. Chem. Soc.*, 2006, **128**, 4970.
31 Y. S. Park, A. C. Whalley, M. Kamenetska, M. L. Steigerwald, M. S. Hybertsen, C. Nuckolls and L. Venkataraman, *J. Am. Chem. Soc.*, 2007, **129**, 15768.
32 S. Y. Quek, M. Kamenetska, M. L. Steigerwald, H. J. Choi, S. G. Louie, M. S. Hybertsen, J. B. Neaton and L. Venkataraman, *Nat. Nanotechnol.*, 2009, **4**, 230.
33 M. Kamenetska, S. Y. Quek, A. C. Whalley, M. L. Steigerwald, H. J. Choi, S. G. Louie, C. Nuckolls, M. S. Hybertsen, J. B. Neaton and L. Venkataraman, *J. Am. Chem. Soc.*, 2010, **132**, 6817.
34 A. Mishchenko, L. A. Zotti, D. Vonlanthen, M. Burkle, F. Pauly, J. C. Cuevas, M. Mayor and T. Wandlowski, *J. Am. Chem. Soc.*, 2011, **133**, 184.
35 R. Parameswaran, J. R. Widawsky, H. Vazquez, Y. S. Park, B. M. Boardman, C. Nuckolls, M. L. Steigerwald, M. S. Hybertsen and L. Venkataraman, *J. Phys. Chem. Lett.*, 2010, **1**, 2114.
36 F. von Wrochem, D. Q. Gao, F. Scholz, H. G. Nothofer, G. Nelles and J. M. Wessels, *Nat. Nanotechnol.*, 2010, **5**, 618.
37 Z. L. Cheng, R. Skouta, H. Vazquez, J. R. Widawsky, S. Schneebeli, W. Chen, M. S. Hybertsen, R. Breslow and L. Venkataraman, *Nat. Nanotechnol.*, 2011, **6**, 353.
38 W. B. Chen, J. R. Widawsky, H. Vazquez, S. T. Schneebeli, M. S. Hybertsen, R. Breslow and L. Venkataraman, *J. Am. Chem. Soc.*, 2011, **133**, 17160.
39 C. A. Martin, D. Ding, J. K. Sorensen, T. Bjornholm, J. M. van Ruitenbeek and H. S. J. van der Zant, *J. Am. Chem. Soc.*, 2008, **130**, 13198.
40 S. T. Schneebeli, M. Kamenetska, Z. L. Cheng, R. Skouta, R. A. Friesner, L. Venkataraman and R. Breslow, *J. Am. Chem. Soc.*, 2011, **133**, 2136.
41 L. Venkataraman, J. E. Klare, I. W. Tam, C. Nuckolls, M. S. Hybertsen and M. L. Steigerwald, *Nano Lett.*, 2006, **6**, 458.
42 E. Leary, M. T. Gonzalez, C. van der Pol, M. R. Bryce, S. Filippone, N. Martin, G. Rubio-Bollinger and N. Agrait, *Nano Lett.*, 2011, **11**, 2236.
43 I. Diez-Perez, J. Hihath, T. Hines, Z. S. Wang, G. Zhou, K. Mullen and N. J. Tao, *Nat. Nanotechnol.*, 2011, **6**, 226.
44 C. Bruot, J. Hihath and N. J. Tao, *Nat. Nanotechnol.*, 2012, **7**, 35.

45 D. P. Long, J. L. Lazorcik, B. A. Mantooth, M. H. Moore, M. A. Ratner, A. Troisi, Y. Yao, J. W. Ciszek, J. M. Tour and R. Shashidhar, *Nat. Mater.*, 2006, **5**, 901.
46 V. Fatemi, M. Kamenetska, J. B. Neaton and L. Venkataraman, *Nano Lett.*, 2011, **11**, 1988.
47 J. H. Liao, J. S. Agustsson, S. M. Wu, C. Schonenberger, M. Calame, Y. Leroux, M. Mayor, O. Jeannin, Y. F. Ran, S. X. Liu and S. Decurtins, *Nano Lett.*, 2010, **10**, 759.
48 C. M. Guédon, H. Valkenier, T. Markussen, K. S. Thygesen, J. C. Hummelen and S. J. van der Molen, *Nat. Nanotechnol.*, 2012, **7**, 305.
49 D. Dulić, S. J. van der Molen, T. Kudernac, H. T. Jonkman, J. J. D. de Jong, T. N. Bowden, J. van Esch, B. L. Feringa and B. J. van Wees, *Phys. Rev. Lett.*, 2003, **91**, 207401.
50 A. C. Whalley, M. L. Steigerwald, X. Guo and C. Nuckolls, *J. Am. Chem. Soc.*, 2007, **129**, 12590.

